

Consistent Diffusion: Denoising Diffusion Model with Data-Consistent Training for Image Restoration

Xinlong Cheng, Tiantian Cao, Guoan Cheng, Bangxuan Huang, Xinghan Tian, Ye Wang, Xiaoyu He,

Weixin Li, Tianfan Xue, Xuan Dong*

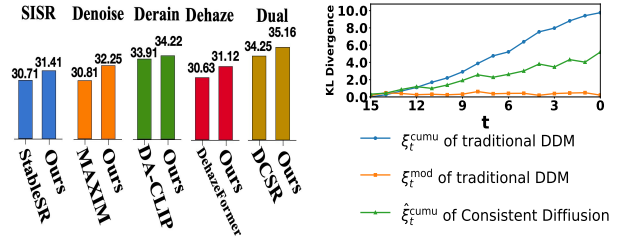
Abstract

In this work, we address the limitations of denoising diffusion models (DDMs) in image restoration tasks, particularly the shape and color distortions that can compromise image quality. While DDMs have demonstrated a promising performance in many applications such as text-to-image synthesis, their effectiveness in image restoration is often hindered by shape and color distortions. We observe that these issues arise from inconsistencies between the training and testing data used by DDMs. Based on our observation, we propose a novel training method, named data-consistent training, which allows the DDMs to access images with accumulated errors during training, thereby ensuring the model to learn to correct these errors. Experimental results show that, across five image restoration tasks, our method has significant improvements over state-of-the-art methods while effectively minimizing distortions and preserving image fidelity.

1. Introduction

The denoising diffusion model (DDM) has demonstrated promising results in various tasks, e.g. text-to-image synthesis, image style transfer, etc. To expand the applications of DDMs, some studies have explored its use in general image restoration tasks, including ResShift [73], Diff-Plugin [34], DiffUIR [82], etc. However, the results of DDMs often exhibit shape and color distortions. While these distortions may be acceptable for entertainment tasks, they significantly degrade image quality in restoration tasks, such as denoising, super-resolution, and dehazing, where high fidelity to the input images is crucial for practical applications like in-camera ISP and image editing software.

To explore the sources of distortions of traditional DDMs, we analyzed their modular error during training and cumulative error during testing at different iterations. As explained in Fig. 2 and [27], the modular error reflects the error of restoring x_t^{train} (the input data during training).



(a) PSNR (dB) values on five tasks. (b) Modular and cumulative errors.

Figure 1. (a) shows PSNR values of the best comparison method and our consistent diffusion on five image restoration tasks: single image super-resolution (SISR), denoise, derain, dehaze, and dual camera super-resolution (Dual). (b) shows that in traditional DDM, the modular error ξ_t^{mod} during training remains low across each iteration t , while the cumulative error ξ_t^{cumu} continuously grows with each testing iteration t . By comparison, in our consistent diffusion, the cumulative error ξ_t^{cumu} during testing remains much lower than ξ_t^{cumu} .

x_t^{train} is generated via the single-step forward processing at iteration t . The cumulative error reflects the error for sequentially running the core network from the first iteration T to the intermediate iteration t . As shown in Fig. 1 (b), there exists a big gap between the modular error during training and the cumulative error during testing. This finding indicates that, while the training focuses on dealing with x_t^{train} , the discrepancies between x_t^{train} and x_t^{test} (the input data during testing) are overlooked. The discrepancies are accumulated to be significant through iterative processing during testing.

Based on our observations, we propose a data-consistent training method. As shown in Fig. 2, at iteration t of the training stage, we align x_t^{train} with x_t^{test} by using backward processing to generate x_t^{train} at each iteration t . This approach minimizes the input differences at any iteration t between training and testing. This ensures that the errors in the testing stage are fully considered during training, and allows the loss optimization in training to directly impact testing accuracy. In addition, to reduce the memory and

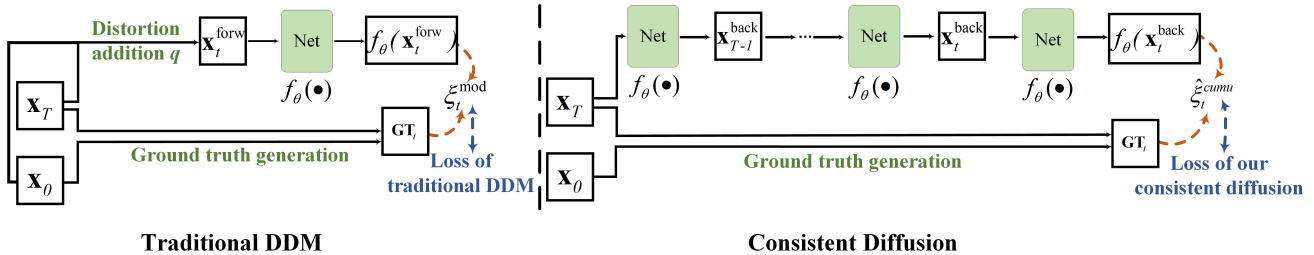


Figure 2. Pipelines of the training methods of traditional DDM vs. our consistent diffusion. At iteration t of the training stage, traditional DDM employs a one-step forward process to obtain the input data $\mathbf{x}_t^{\text{train}}$, i.e. $\mathbf{x}_t^{\text{train}} = \mathbf{x}_t^{\text{forw}} \sim q(\mathbf{x}_t | \mathbf{x}_0)$, where q is the distortion addition operation. The training loss, which measures the quality of $f_\theta(\mathbf{x}_t^{\text{forw}})$, is optimizing the modular error ξ_t^{mod} of the core network while failing to take the input cumulative error into consideration. f_θ is the processing of the core network with the parameter θ . In contrast, our consistent diffusion proposes the data-consistent training. It utilizes the multi-step backward process, which is consistent with that in the testing stage, to generate the input data $\mathbf{x}_t^{\text{train}}$ at iteration t , i.e. $\mathbf{x}_t^{\text{train}} = \mathbf{x}_t^{\text{back}} \sim p_\theta(\mathbf{x}_T) \prod_{i=T}^{t+1} p_\theta(\mathbf{x}_{i-1} | \mathbf{x}_i)$. p_θ denotes the denoising process parameterized by θ . The training loss, which measures the quality of $f_\theta(\mathbf{x}_t^{\text{back}})$, is directly optimizing the cumulative error $\hat{\xi}_t^{\text{cumu}}$ of the core network.

computational cost of data-consistent training, we also provide an efficient version with a certain bias.

In our experiments, we select ResShift [73] as the backbone DDM, one of the state-of-the-art (SOTA) models with minimal diffusion steps, and apply the proposed data-consistent training method to train the model. We evaluate the method on five popular image restoration tasks: single-image super-resolution, denoising, deraining, dehazing, and dual-camera super-resolution. Training is performed using a single NVIDIA A6000 GPU. The results in Fig. 1 and Sec. 5 show that our method achieves SOTA accuracy compared to other methods and produces high-fidelity outputs that effectively prevent color and shape distortions.

Our contributions can be summarized as follows. (1) We propose the data-consistent training method to mitigate error propagation during the iterative processing of DDM. (2) The proposed method is applicable to any DDM backbone and can be used for various image restoration tasks. (3) Experiments across five image restoration tasks demonstrate that our method achieves SOTA accuracy while effectively preventing distortions.

2. Related Work

2.1. Restoration methods.

Before the deep learning era, there exist various miles-stone non-deep solutions, e.g. sparse coding for image super resolution [68], non-local means for image denoising [9], dark channel prior for image dehaze [15], etc.

Among deep learning methods, CNN is widely used in different restoration tasks, including SISR [22, 31, 76, 77], denoising [23], deblurring [1, 10, 38], derain [12, 13, 84], dehaze [7, 8, 41], and dual-camera super resolution [55, 72, 80]. With the increase of data and computation resources, Transformer becomes a more powerful backbone

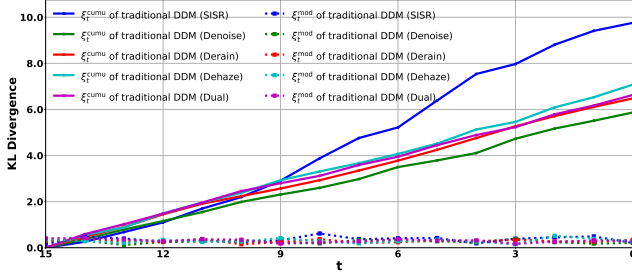
than CNN. Some works solve multiple restoration tasks, e.g. Pretrained-IPT [3], Restormer [74], U-Former [58], CSformer [69], SwinIR [30], PromptRestorer [53], GRL [29], and there also exist many specifically designed models for single tasks, including SISR [5, 30, 83], denoising [65], deblurring [29, 49, 50], derain [26, 52, 64], dehaze [6, 14, 28], and reference-based super resolution [67].

2.2. Denoising Diffusion Models.

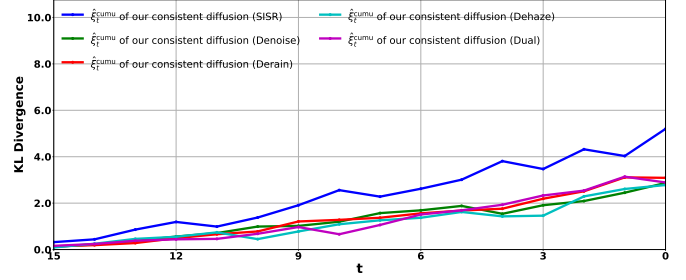
Denoising Diffusion Models (DDMs) (e.g. DDPM [16], DDIM [45], LDM [42]) provide a more complicated and powerful backbone in the computer vision field. In a wide range of tasks like text-to-image synthesis and image generation with multimodal inputs, DDMs have shown promising results, e.g. ControlNet [75], Uni-controlnet [81], smol-imagen [43], Improved-NAT [39], Splatter image [48], Diffusion-distiller [44].

DDMs have also been studied to serve for image restoration. Some works try to design the model for various restoration tasks, e.g. GenerativeDiffusionPrior [11], DiffIR [63], DiffPIR [85], DiffUIR [82], Diff-Plugin [34], FlowIE [86], TextualDegRemoval [32], and DTPM [70]. The other works focus on dealing with a single task, like single image super-resolution [54, 57, 62, 71, 73] and image deblurring, e.g. DSR [60] and ID-Blau [61].

The existing DDM methods provide a variety of ways to revise the network structure and add pre-/post-processing subnets to improve the accuracy of DDMs for image restoration. We notice that the training and testing strategy of most of these DDMs follows the traditional DDPM and DDIM. However, the cumulative error through the iterative processing of DDMs during testing is not considered in the training stage, leading to uncontrolled errors which could decrease the fidelity and accuracy much a lot.



(a) ξ_t^{mod} and ξ_t^{cumu} of traditional DDM on five restoration tasks.



(b) $\hat{\xi}_t^{cumu}$ of our consistent diffusion on five restoration tasks.

Figure 3. (a) shows the statistics of traditional DDM across five tasks, revealing a persistent gap between the modular error ξ_t^{mod} , which is minimized by the loss function during training, and the cumulative error ξ_t^{cumu} , which represents the true error during testing. We use ResShift [73] as the traditional DDM here. In contrast, (b) shows that the cumulative errors $\hat{\xi}_t^{cumu}$ of our consistent diffusion are significantly lower than cumulative errors ξ_t^{cumu} of traditional DDM in (a), benefiting from our data-consistent training which directly optimizes for cumulative error reduction. Our consistent diffusion uses the backbone of ResShift with the proposed data-consistent training.

3. Preliminaries

3.1. Error analysis

DDM is a sequence model which iteratively process the input data from low quality to high quality step-by-step to obtain the final output. As mentioned in [27] and explained in Fig. 3, at iteration t , there exists the **modular error** and **cumulative error**.

Modular error ξ_t^{mod} measures the accuracy of the output of the core network given an input \mathbf{x}_t at iteration t , i.e.

$$\xi_t^{mod} = D(f_\theta(\mathbf{x}_t), \mathbf{GT}_t), \quad (1)$$

where D denotes the metric to measure the differences of the pair of images and we follow [27] to use KL divergence as the metric, f_θ denotes the process of the core network, and \mathbf{GT}_t is ground truth image at iteration t .

Cumulative error ξ_t^{cumu} measures the amount of error that are accumulated for sequentially running the core network from the first iteration T to the current iteration t . The error comes from the modular error and the input cumulative error, i.e.

$$\xi_t^{cumu} = \xi_t^{mod} + \mu_t \xi_{t+1}^{cumu}, \quad (2)$$

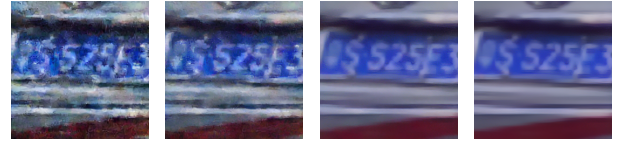
where μ_t specifies how much the input cumulative error ξ_{t+1}^{cumu} is propagated to ξ_t^{cumu} . The input error is defined as

$$\xi_{t+1}^{cumu} = D(\mathbf{x}_t^{back}, \mathbf{x}_t), \quad (3)$$

where \mathbf{x}_t^{back} is the input data at iteration t according to the backward process. \mathbf{x}_t^{back} is obtained by linking the computation of all the previous iterations, i.e. $\mathbf{x}_t^{back} \sim p_\theta(\mathbf{x}_T) \prod_{i=T}^{t+1} p_\theta(\mathbf{x}_{i-1} | \mathbf{x}_i)$, where $p_\theta(x_{t-1} | x_t)$ denotes the processing of the core network with the parameter θ shared across different iterations. As proved in [27], we have $\mu_t \geq 1$. This means that the input cumulative error is at least fully spread to the next iteration, and the cumulative errors cannot be neglected.



(a) Intermediate results of selected iterations in training of traditional DDM



(b) Intermediate results of selected iterations in testing of traditional DDM



(c) Intermediate results of selected iterations in training of our consistent diffusion



(d) Intermediate results of selected iterations in testing of our consistent diffusion

Figure 4. In traditional DDM, the gap of training and testing in (a) and (b) shows that although the modular error is minimized well during training, cumulative errors are not well controlled during testing. (c) and (d) show consistent accuracy between training and testing of our consistent diffusion, and demonstrate the effectiveness of our method to reduce cumulative errors during testing by optimizing them during training.

3.2. Traditional DDM

In the training stage of traditional DDMs, at each iteration t , the input data $\mathbf{x}_t^{\text{train}}$ is usually generated according to

the forward processing, i.e. $\mathbf{x}_t^{\text{train}} = \mathbf{x}_t^{\text{forw}}$. $\mathbf{x}_t^{\text{forw}}$ is obtained by the one-step distortion addition operation q , i.e. $\mathbf{x}_t^{\text{forw}} \sim q(\mathbf{x}_t | \mathbf{x}_0)$, where \mathbf{x}_0 is the ground-truth image. The loss function in the training stage of traditional DDMs is usually designed as

$$Loss = \sum_t \beta_t(f_\theta(\mathbf{x}_t^{\text{train}}), \mathbf{GT}_t) = \sum_t \beta_t(f_\theta(\mathbf{x}_t^{\text{forw}}), \mathbf{GT}_t), \quad (4)$$

where β_t is the metric at iteration t . This actually minimizes the modular error according to Eq. 1.

However, in the testing stage where the backward process is performed, according to the cumulative error in Eq. 2, there exist two error sources, i.e. modular error ξ_t^{mod} and input cumulative error $\mu_t \xi_{t+1}^{\text{cumu}}$. The loss function in Eq. 4 does not consider the cumulative error at all. During the training, the modular error can hardly be minimized to zero at each iteration. Since $\mu_t \geq 1$, the cumulative error will increase through the series of iterations and cannot be neglected, as shown in Figs. 1 and 3. Failing to consider the cumulative error in the training stage leads to uncontrolled errors into the testing stage and the accuracy gap between the training stage and the testing stage of traditional DDM, as shown in Figs. 1 and 3.

4. Method

4.1. Data-Consistent Training

We notice that the limitation of the training method of traditional DDMs comes from the data inconsistency, i.e. the input data in the training stage is $\mathbf{x}_t^{\text{forw}}$, while that in the testing stage is $\mathbf{x}_t^{\text{back}}$.

At iteration t of the training stage, we let the input change from $\mathbf{x}_t^{\text{forw}}$ to $\mathbf{x}_t^{\text{back}}$, i.e. $\mathbf{x}_t^{\text{train}} = \mathbf{x}_t^{\text{back}}$, to avoid the data inconsistency. In this way, according to Eq. 1, the new modular error changes to

$$\hat{\xi}_t^{\text{mod}} = D(f_\theta(\mathbf{x}_t^{\text{train}}), \mathbf{GT}_t) = D(f_\theta(\mathbf{x}_t^{\text{back}}), \mathbf{GT}_t), \quad (5)$$

and, according to Eq. 3, the input cumulative error changes to

$$\hat{\xi}_{t+1}^{\text{cumu}} = D(\mathbf{x}_t^{\text{back}}, \mathbf{x}_t^{\text{train}}) = D(\mathbf{x}_t^{\text{back}}, \mathbf{x}_t^{\text{back}}) = 0. \quad (6)$$

Thus, according to Eq. 2, the cumulative error is

$$\hat{\xi}_t^{\text{cumu}} = \hat{\xi}_t^{\text{mod}} + \mu_t \cdot 0 = \hat{\xi}_t^{\text{mod}}. \quad (7)$$

This indicates that by using $\mathbf{x}_t^{\text{back}}$ as the input, the cumulative error at iteration t is only decided by $\hat{\xi}_t^{\text{mod}}$ and there does not exist any other error sources. Thus, we can follow traditional DDM to design the loss function to only measure the modular error, i.e.

$$Loss = \sum_t \beta_t(f_\theta(\mathbf{x}_t^{\text{train}}), \mathbf{GT}_t) = \sum_t \beta_t(f_\theta(\mathbf{x}_t^{\text{back}}), \mathbf{GT}_t), \quad (8)$$

where β_t is the metric at iteration t .

Method	PSNR (\uparrow)	SSIM (\uparrow)	LPIPS (\downarrow)	FID (\downarrow)	CLPIQA (\uparrow)
DA-CLIP [37]	29.67	0.8272	0.1262	128.28	0.1075
SwinIR [30]	29.82	0.8711	0.2293	197.59	<u>0.1973</u>
AirNet [25]	28.88	0.8702	0.2108	141.13	0.1129
DiffPlugin [34]	23.65	0.7901	0.1442	141.75	0.0826
DiffUIR [82]	24.69	0.8166	0.1863	<u>76.03</u>	0.0766
PromptIR [40]	29.39	<u>0.8810</u>	0.1291	166.38	0.1206
Restormer [74]	30.02	0.8316	<u>0.1030</u>	115.24	0.1249
MAXIM [51]	<u>30.81</u>	0.9030	0.1362	195.92	0.1498
Blind2Unblind [59]	25.32	0.7366	0.2189	179.99	0.1018
KBNet [78]	30.04	0.8753	0.2546	128.43	<u>0.2073</u>
Pretrained-IPT [3]	29.71	0.8178	0.2874	208.46	0.1603
SADNet [47]	27.92	0.8332	<u>0.1159</u>	116.97	0.1186
Ours (efficient)	30.42	0.8784	0.1589	<u>63.97</u>	0.1620
Ours	32.25	<u>0.8989</u>	0.0812	61.82	0.2090

Table 1. Quantitative comparison of denoising on Urban100 [17]. We compare 8 general and 4 task-specific restoration models.

4.2. Efficient Data-Consistent Training

Although the proposed data-consistent training ensures no input cumulative error, it can lead to a increase in memory and computation costs in the training stage, because the input at each iteration t , i.e. $\mathbf{x}_t^{\text{back}}$, needs to be generated by the series process of the core network from iteration T to iteration $t + 1$.

For users that require low memory and computation costs in the training stage, we provide the alternative efficient version of our method, with the cost of small image quality drops. We introduce a two-step approach for generating the input at iteration t , named $\tilde{\mathbf{x}}_t^{\text{train}}$. First, we generate $\tilde{\mathbf{x}}_{t+1}^{\text{train}}$, i.e. the input data at iteration $t + 1$, using the forward process. It is obtained by $\tilde{\mathbf{x}}_{t+1}^{\text{train}} = \mathbf{x}_{t+1}^{\text{forw}}$, and $\mathbf{x}_{t+1}^{\text{forw}} \sim q(\mathbf{x}_{t+1} | \mathbf{x}_0)$. Next, we use f_θ to obtain the processing result of iteration $t + 1$, i.e. $f_\theta(\tilde{\mathbf{x}}_{t+1}^{\text{train}})$. In this context, we have already introduced one-step cumulative error into $f_\theta(\tilde{\mathbf{x}}_{t+1}^{\text{train}})$. The one-step error \mathbf{e} is calculated by

$$\mathbf{e} = f_\theta(\tilde{\mathbf{x}}_{t+1}^{\text{train}}) - \mathbf{GT}_{t+1}. \quad (9)$$

To simulate the cumulative errors during testing, we assume μ_t in Eq. 2 is equal to 1 at each iteration. To ensure the strength of error is the same with that in consistent diffusion, we amplify the one-step error \mathbf{e} by λ times, and set $\lambda = T - t$ according to the number of iterations to obtain $\tilde{\mathbf{x}}_t^{\text{train}}$, i.e.

$$\tilde{\mathbf{x}}_t^{\text{train}} = f_\theta(\tilde{\mathbf{x}}_{t+1}^{\text{train}}) + \lambda \cdot \mathbf{e}, \quad (10)$$

and the loss function changes to

$$Loss = \sum_t \beta_t(f_\theta(\tilde{\mathbf{x}}_t^{\text{train}}), \mathbf{GT}_t). \quad (11)$$

5. Experiments

5.1. Datasets and Implementation Details.

Datasets. We conduct experiments across five tasks: single image super-resolution (SISR), denoising, deraining, de-

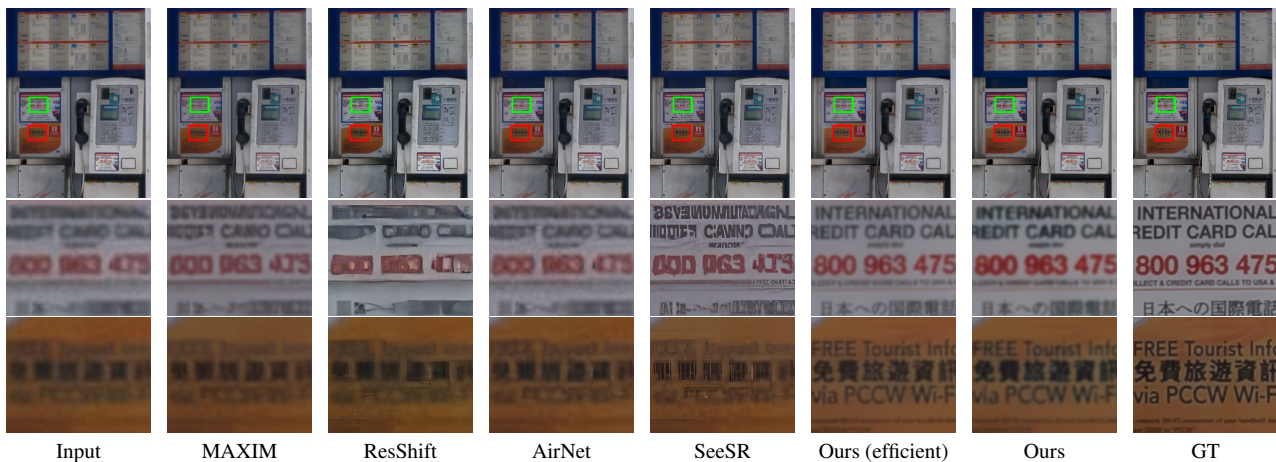


Figure 5. Example results in single image super-resolution on RealSR. The marked regions are enlarged. Due to page limits, we show results of the top 4 comparison methods here. Complete results and additional comparisons are available in the supplementary materials.

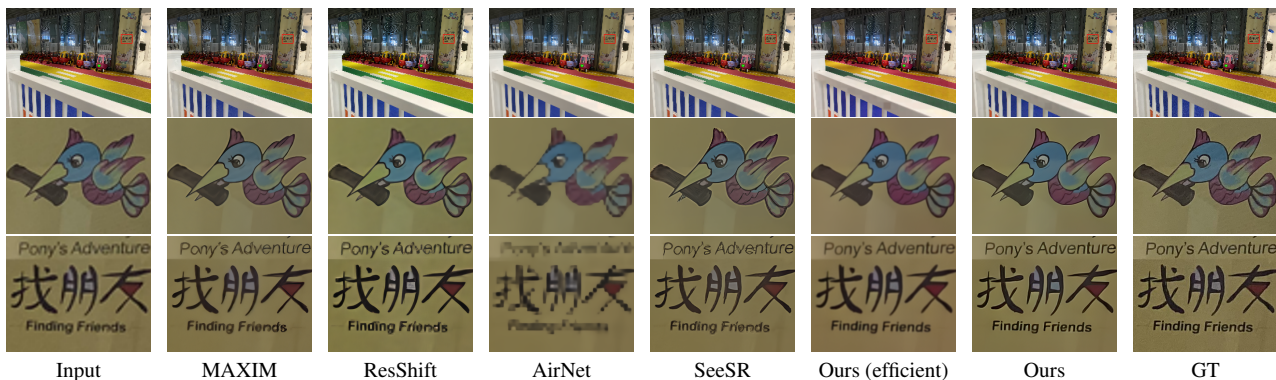


Figure 6. Example results in single image super-resolution on CameraFusion. Please see more results in the supplementary materials.

Method	PSNR (\uparrow)	SSIM (\uparrow)	LPIPS (\downarrow)	FID (\downarrow)	CLIPQA (\uparrow)
DA-CLIP [37]	<u>33.91</u>	<u>0.9261</u>	<u>0.0942</u>	48.28	0.1239
SwinIR [30]	25.22	0.8369	0.2621	123.28	0.0791
AirNet [25]	19.34	0.6734	0.3336	221.33	0.0878
DiffPlugin [34]	22.71	0.7371	0.2002	188.15	0.1066
DiffUIR [82]	19.66	0.6742	0.3019	217.10	0.0858
PromptIR [40]	20.76	0.6828	0.2792	190.93	0.0963
Restormer [74]	<u>31.46</u>	0.9043	0.1289	111.03	0.1297
MAXIM [51]	28.25	0.8963	0.1397	112.48	0.1258
WGWS [84]	20.15	0.6678	0.2901	285.95	0.0648
KBNet [78]	29.13	0.8991	0.1362	114.43	<u>0.1335</u>
Pretrained-IPT [3]	20.28	0.6925	0.3385	224.95	0.1193
Ours (efficient)	31.08	<u>0.9219</u>	<u>0.1117</u>	<u>56.63</u>	<u>0.1510</u>
Ours	34.22	0.9359	0.0747	<u>98.85</u>	0.2276

Table 2. Quantitative comparison of derain on Rain-100H [19]. We compare 8 general and 3 task-specific restoration models.

hazing, and dual-camera super-resolution. For SISR experiment, we adopt the 4x upscaling task. We utilize DIV2K [2] and Flickr2K [2] datasets for training, and RealSR [18] dataset and CameraFusion [55] dataset for testing. For denoising, we follow [30, 40] to leverage the training set of SIDD [33] dataset for training, and Urban100 [17] dataset for testing, where random Gaussian noise with a standard

Method	PSNR (\uparrow)	SSIM (\uparrow)	LPIPS (\downarrow)	FID (\downarrow)	CLIPQA (\uparrow)
DA-CLIP [37]	<u>30.42</u>	<u>0.9668</u>	<u>0.0341</u>	6.76	0.1373
SwinIR [30]	25.11	0.8314	0.1282	44.89	0.1381
AirNet [25]	22.39	0.8630	0.1363	30.45	0.1457
DiffPlugin [34]	24.60	0.8752	0.1069	32.26	0.1291
DiffUIR [82]	25.76	0.8609	0.1579	68.72	0.1889
PromptIR [40]	26.79	0.8214	0.1307	23.39	0.1447
Restormer [74]	28.81	0.9537	0.0460	9.16	0.1328
MAXIM [51]	26.04	0.9360	0.0456	<u>7.21</u>	0.1591
mixDehazeNet [36]	29.13	0.9547	0.0513	46.53	0.1688
dehazeFormer [46]	<u>30.63</u>	<u>0.9741</u>	<u>0.0379</u>	9.21	0.1386
WGWS [84]	21.78	0.8472	0.1645	93.20	<u>0.1698</u>
Ours (efficient)	29.19	0.9309	0.1156	16.68	0.1604
Ours	31.12	0.9747	0.0321	<u>7.43</u>	<u>0.1860</u>

Table 3. Quantitative comparison of dehaze on RESIDE-6k [24]. We compare 8 general and 3 task-specific restoration models.

deviation of 50 is added to high-quality images to obtain the input images. For deraining, we adopt Rain-13k [19] dataset for training, and Rain-100H [19] dataset for testing. For dehazing, we use the training set of RESIDE-6k [24] dataset for training, and the testing set of RESIDE-6k dataset for testing. For dual-camera super-resolution, we incorporate the training set of the CameraFusion dataset for

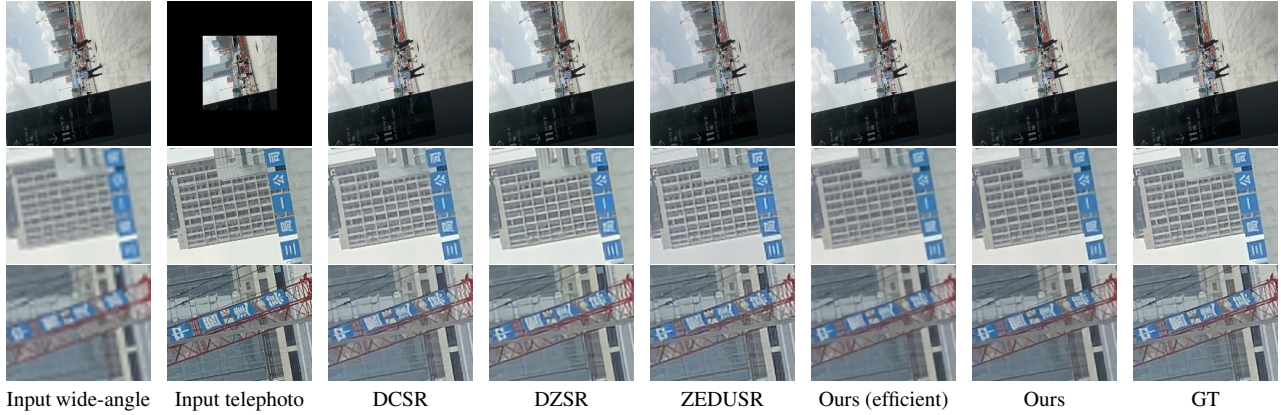


Figure 7. Example results in dual-camera super resolution on CameraFusion. Please see more results in supplementary materials.

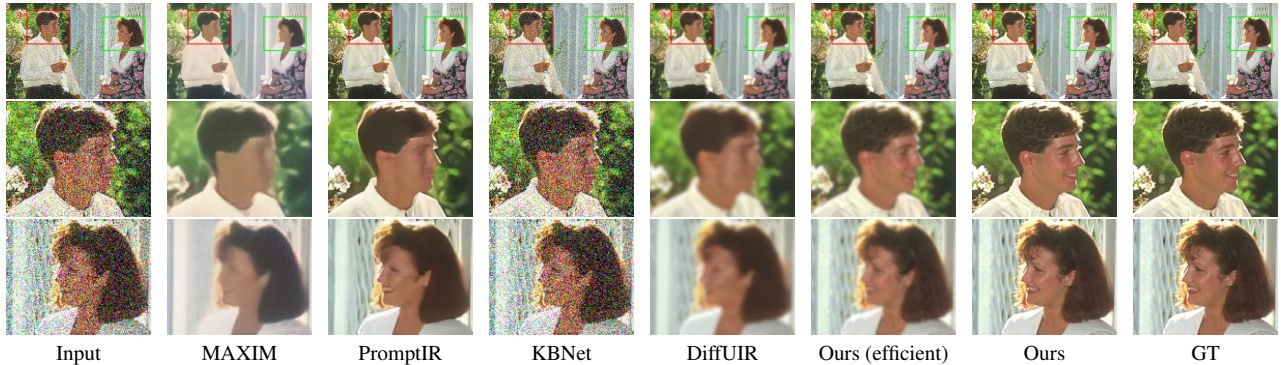


Figure 8. Example results in image denoising on Urban100. Please see more results in supplementary materials.

Method	PSNR (\uparrow)	SSIM (\uparrow)	LPIPS (\downarrow)	FID (\downarrow)	CLIQQA (\uparrow)
SwinIR [30]	25.99	0.7657	0.1164	25.04	0.0733
ZEDUSR [66]	30.28	0.8976	0.0334	10.22	0.0864
C ² -Matching [20]	31.79	0.8264	0.0417	14.75	0.0773
DCSR [55]	34.25	0.8785	0.0263	8.78	0.0839
DZSR [80]	31.39	0.8602	0.0820	18.87	0.1042
EDSR [72]	32.35	0.6543	0.0295	17.57	0.0778
MASA [35]	29.94	0.8041	0.0763	18.63	0.0892
RCAN [66]	32.45	0.8555	0.0293	18.46	0.0783
Real-ESRGAN [56]	27.80	0.7660	0.1637	28.91	0.0889
SRGAN [21]	29.27	0.7622	0.0935	14.96	0.0852
SRNTT [79]	31.42	0.8224	0.0449	17.76	0.0756
TTSR [67]	29.13	0.7767	0.0498	14.75	0.0874
Ours (efficient)	33.78	0.8760	0.0535	18.59	0.0873
Ours	35.16	0.9047	0.0158	7.43	0.0860

Table 4. Quantitative comparison of dual camera super-resolution on CameraFusion [55]. We compare 12 task-specific methods.

training, and the testing set of CameraFusion dataset for testing. We follow ZEDUSR [72] to bicubic downsample the wide-angle images by a factor of 4 to obtain the input, while the original wide-angle images serve as the target images and the telephoto images act as references.

Implementations of Our Method. Our method uses Resshift as the backbone DDM due to its efficiency. The ground-truth image $\mathbf{GT} = \mathbf{x}_0$, the input low-quality image is \mathbf{y}_0 , and the residue $\mathbf{r}_0 = \mathbf{y}_0 - \mathbf{x}_0$. At iteration t , the

ground-truth image $\mathbf{GT}_t = \mathbf{x}_0 + \eta_{t-1}\mathbf{r}_0$. In the forward process, the distortion addition operation at iteration t is defined as $q(\mathbf{x}_t|\mathbf{x}_0)$, and $q(\mathbf{x}_t|\mathbf{x}_0) = \mathcal{N}(\mathbf{x}_t; \mathbf{x}_0 + \eta_t\mathbf{r}_0, \kappa^2\eta_t\mathbf{I})$, where $\{\eta_t\}$ is a shifting sequence which monotonically increases with the iteration t , κ is a hyper-parameter, and \mathbf{I} is the identity matrix.

In the experiments, we use a single NVIDIA A6000 GPU with a total batch size of 4. We employ a cosine learning rate scheduler, setting a maximum learning rate of 1×10^{-4} . Additionally, we implement exponential moving average (EMA) to enhance training stability and overall model performance. All the training is carried out at a resolution of 256×256 , with mean square error (MSE) as the metric β_t of the loss function.

Comparison Methods. We prioritize comparing the SOTA general restoration models, including the CNN based methods of AirNet, the transformer based methods of DA-CLIP, MAXIM, PromptIR, Restormer and SwinIR, and the DDM based methods of DiffPlugin and DiffUIR. In addition, we also compare the SOTA models for each task. For SISR, we compare Real-ESRGAN, HAT, Resshift, SeeSR, SRFormer and DiffIR. For denoising, we compare Blind2UnBlind, Pretrained-IPT and SADNet. For deraining, we compare Pretrained-IPT, WGWS and KBNNet. For

Method	RealSR					CameraFusion				
	PSNR (\uparrow)	SSIM (\uparrow)	LPIPS (\downarrow)	FID (\downarrow)	CLIPQA (\uparrow)	PSNR (\uparrow)	SSIM (\uparrow)	LPIPS (\downarrow)	FID (\downarrow)	CLIPQA (\uparrow)
DA-CLIP [37]	25.24	0.7532	0.3639	116.22	0.2054	21.54	0.7554	0.1450	42.34	0.0873
SwinIR [30]	24.58	0.7477	0.3605	102.18	0.1934	26.98	0.7473	0.1597	35.21	0.0807
AirNet [25]	26.03	<u>0.7611</u>	0.3556	111.35	0.1993	26.15	0.7974	0.1539	35.72	0.0889
DiffPlugin [34]	24.59	0.7431	0.3797	102.10	0.2003	29.86	0.7901	0.1442	31.75	0.0862
DiffUIR [82]	25.23	<u>0.7612</u>	0.3681	129.48	<u>0.2076</u>	29.40	0.7966	0.0621	46.03	0.0764
PromptIR [40]	20.47	0.7437	0.3327	149.86	0.2223	26.08	0.6915	0.1286	31.03	0.0890
Restormer [74]	<u>25.91</u>	0.7315	0.3533	116.48	0.2060	30.35	<u>0.8365</u>	0.0269	29.23	0.0799
MAXIM [51]	21.26	0.7415	0.3660	105.86	0.2059	22.72	0.7490	0.1742	89.54	0.0493
Real-ESRGAN [56]	24.27	0.7432	0.3658	104.87	0.1953	27.48	0.7619	0.1575	40.66	0.0921
DiffIR [63]	25.68	0.7772	0.3461	105.48	0.1892	30.36	0.8051	0.1382	34.08	0.0815
HAT [4]	25.86	0.7552	0.3581	110.26	0.2001	29.40	0.7966	<u>0.0601</u>	45.93	0.0765
ResShift [73]	24.59	0.7431	0.3797	102.10	0.1903	27.28	0.7824	0.1332	28.58	0.0765
SeeSR [62]	24.79	0.7246	0.3597	79.64	0.1912	28.42	0.7674	0.1488	<u>28.31</u>	0.0891
StableSR [54]	25.81	0.7401	0.4586	84.53	0.1961	30.71	<u>0.8268</u>	0.1561	44.29	0.1181
SRFormer [83]	24.87	0.7562	0.3567	96.19	0.1712	28.60	0.7871	0.1511	35.54	0.0764
Ours (efficient)	25.09	0.7430	<u>0.3453</u>	<u>89.52</u>	0.1899	28.68	0.7965	0.1767	59.85	<u>0.1123</u>
Ours	<u>25.96</u>	0.7471	<u>0.3402</u>	99.02	0.1957	31.41	0.8391	<u>0.0427</u>	27.64	<u>0.1006</u>

Table 5. Quantitative comparison of single image super-resolution on RealSR [18] and CameraFusion [55].



Figure 9. Example results in image deraining on Rain-100H. Please see more results in supplementary materials.

Method	Dataset	PSNR (\uparrow)	SSIM (\uparrow)	LPIPS (\downarrow)	FID (\downarrow)	CLIPQA (\uparrow)
ResShift [73]	RealSR	24.59	0.7431	<u>0.3797</u>	102.10	<u>0.1903</u>
LDM [42]	RealSR	<u>25.19</u>	<u>0.7586</u>	<u>0.3691</u>	111.88	0.1208
$L_{ntt} + L_{reg}$ [27]	RealSR	24.71	0.7289	0.4072	75.89	0.0996
LDM+DCT	RealSR	27.60	0.7821	0.3909	86.49	<u>0.1905</u>
ResShift+DCT (Ours)	RealSR	<u>25.96</u>	<u>0.7471</u>	0.3402	<u>99.02</u>	0.1957
ResShift [73]	CameraFusion	27.28	<u>0.7824</u>	<u>0.1332</u>	<u>28.58</u>	0.0765
LDM [42]	CameraFusion	26.15	0.7465	0.2211	<u>44.13</u>	0.1317
$L_{ntt} + L_{reg}$ [27]	CameraFusion	<u>30.23</u>	0.7425	<u>0.0821</u>	56.90	0.0859
LDM+DCT	CameraFusion	<u>28.68</u>	<u>0.7965</u>	0.1767	59.85	<u>0.1123</u>
ResShift+DCT (Ours)	CameraFusion	31.41	0.8391	0.0427	27.64	<u>0.1006</u>

Table 6. Ablation study about our data-consistent training. ‘DCT’ is short for the proposed data-consistent training.

Method	Dataset	PSNR (\uparrow)	SSIM (\uparrow)	LPIPS (\downarrow)	FID (\downarrow)	CLIPQA (\uparrow)
No amplification	RealSR	22.74	0.7339	0.4115	104.67	0.1208
Random amplification	RealSR	23.35	0.7368	0.3929	114.39	0.2136
Ours (efficient)	RealSR	25.09	0.7430	0.3453	89.52	0.1899
No amplification	CameraFusion	22.95	0.6614	0.3418	148.73	0.1498
Random amplification	CameraFusion	27.61	0.7513	0.1979	61.08	0.1170
Ours (efficient)	CameraFusion	28.68	0.7965	0.1767	59.85	0.1123

Table 7. Ablation study about the efficient version of our method.

dehazing, we compare mixDehazeNet, dehazeFormer and WGWS. Dual-camera super-resolution is a special task, and we compare SwinIR, ZEDUSR, C²-Matching, DCSR, DZSR, EDSR, MASA, RCAN, Real-ESRGAN, SRGAN,

Memory/Time costs	ResShift (T=15)	Ours (T=15)	Ours efficient (T=15)
Train (256*256)	16.5GB/27h	41.7GB/90h	19.8GB/28h
Test (256*256)	3.6GB/0.96s	3.6GB/0.96s	3.6GB/0.96s
Test (1024*1024)	14.1GB/13s	14.1GB/13s	14.1GB/13s

Table 8. Computational costs of ResShift, our method, and our efficient version in training and testing stages. ‘h’ and ‘s’ are short for hours and seconds respectively.

SRNTT and TTSR. We retrain the models based on the author’s provided code if there are no released model weights.

5.2. Results and analysis.

The quantitative results of five tasks are shown in Tables 1, 2, 3, 4 and 5. The qualitative results of five tasks are shown in Figs. 5, 6, 7, 8, 9 and 10. Our results not only achieve high naturalness quality but also show high fidelity quality to the input without shape and color distortions. In the five tasks, our method usually achieves the best or top-three accuracy across various metrics. In contrast, other compared algorithms exhibit greater variability in accuracy across different test datasets and metrics. This indicates that our algorithm not only delivers strong results but also



Figure 10. Example results in image dehaze on RESIDE-6k. Please see more results in supplementary materials.



Figure 11. Example results of the ablation study about our data-consistent training. ‘DCT’ is short for the proposed data-consistent training.

demonstrates robust generalization capabilities. In dual-camera super-resolution, SOTA comparison methods like DCSR often require complex architectures with multiple sub-networks to address challenges such as motion alignment, occlusion, and tonal inconsistencies between the input and reference images. In contrast, our method achieves SOTA accuracy without relying on specialized subnet designs or additional pre-/post-processing steps. This superior performance highlights the robust learning capacity of our model, which not only effectively learns the mapping from low-quality to high-quality but also is capable of addressing a variety of compound problems without the need for task-specific architectural modifications.

Ablation Study. We try different variants of the proposed method. (1) To evaluate the benefits of our data-consistent training vs. the traditional training for different DDM backbones, besides ResShift, we also use latent diffusion model (LDM) as the backbone. Their results with the traditional training are denoted as ResShift and LDM, and their results with our data-consistent training are denoted as ResShift+DCT and LDM+DCT. (2) The work [27] also notices the gap between modular error and cumulative error and propose to use $L_{nll} + L_{reg}$ to train the DDM backbone, where $L_t^{nll} = \beta_t(f_\theta(\mathbf{x}_t^{forw}), \mathbf{GT}_t)$ follows the traditional DDM, $L_t^{reg} = \beta_t(f_\theta(\mathbf{x}_t^{back}), \mathbf{x}_{t-1}^{forw})$ L_{nll} pushes the out-

put the same as the image generated by forward process. We also use ResShift as the backbone.

We also try different possible variants about our efficient version. (1) We follow Li et al. [27] to use the forward process to generate $\mathbf{x}_{t+1}^{train} = \mathbf{x}_{t+1}^{forw}$, and use two times f_θ to process it to get the output at iteration t without error amplification, denoted as ‘No amplification’. (2) We also try to use a random value between 0 and $(T - t)$ to amplify the error, denoted as ‘Random amplification’.

The results in Tables 6, 7 and Fig. 11 show the advantage of our choices and the generalizability of the proposed data-consistent training for different DDM backbones.

6. Conclusions

We address the limitations of traditional DDMs in image restoration by proposing a data-consistent training method to avoid shape and color distortions of the results. This method aligns the input data across both training and testing stages, ensuring that errors accumulated during testing are taken into consideration during training. Using ResShift as our backbone DDM, we achieve state-of-the-art accuracy on five popular image restoration tasks while maintaining high fidelity. Our method provides a general training solution for DDMs across various restoration tasks.

References

- [1] Abdullah Abuolaim and Michael S Brown. Defocus deblurring using dual-pixel data. In *Computer Vision—ECCV 2020: 16th European Conference, Glasgow, UK, August 23–28, 2020, Proceedings, Part X 16*, pages 111–126. Springer, 2020. 2
- [2] Eirikur Agustsson and Radu Timofte. Ntire 2017 challenge on single image super-resolution: Dataset and study. In *Proceedings of the IEEE conference on computer vision and pattern recognition workshops*, pages 126–135, 2017. 5
- [3] Hanting Chen, Yunhe Wang, Tianyu Guo, Chang Xu, Yiping Deng, Zhenhua Liu, Siwei Ma, Chunjing Xu, Chao Xu, and Wen Gao. Pre-trained image processing transformer. In *Proceedings of the IEEE/CVF conference on computer vision and pattern recognition*, pages 12299–12310, 2021. 2, 4, 5
- [4] Xiangyu Chen, Xintao Wang, Wenlong Zhang, Xiangtao Kong, Yu Qiao, Jiantao Zhou, and Chao Dong. Hat: Hybrid attention transformer for image restoration. *arXiv preprint arXiv:2309.05239*, 2023. 7
- [5] Xiangyu Chen, Xintao Wang, Jiantao Zhou, Yu Qiao, and Chao Dong. Activating more pixels in image super-resolution transformer. In *Proceedings of the IEEE/CVF conference on computer vision and pattern recognition*, pages 22367–22377, 2023. 2
- [6] Zixuan Chen, Zewei He, and Zhe-Ming Lu. Dea-net: Single image dehazing based on detail-enhanced convolution and content-guided attention. *IEEE Transactions on Image Processing*, 2024. 2
- [7] Yuning Cui, Wenqi Ren, Sining Yang, Xiaochun Cao, and Alois Knoll. Innext: Rethinking convolutional network design for image restoration. In *International conference on machine learning*, 2023. 2
- [8] Yuning Cui, Wenqi Ren, and Alois Knoll. Omni-kernel network for image restoration. In *Proceedings of the AAAI Conference on Artificial Intelligence*, pages 1426–1434, 2024. 2
- [9] Kostadin Dabov, Alessandro Foi, Vladimir Katkovnik, and Karen Egiazarian. Image denoising by sparse 3-d transform-domain collaborative filtering. *IEEE Transactions on image processing*, 16(8):2080–2095, 2007. 2
- [10] Zhenxuan Fang, Fangfang Wu, Weisheng Dong, Xin Li, Jinjian Wu, and Guangming Shi. Self-supervised non-uniform kernel estimation with flow-based motion prior for blind image deblurring. In *Proceedings of the IEEE/CVF conference on computer vision and pattern recognition*, pages 18105–18114, 2023. 2
- [11] Ben Fei, Zhaoyang Lyu, Liang Pan, Junzhe Zhang, Weidong Yang, Tianyue Luo, Bo Zhang, and Bo Dai. Generative diffusion prior for unified image restoration and enhancement. In *Proceedings of the IEEE/CVF Conference on Computer Vision and Pattern Recognition*, pages 9935–9946, 2023. 2
- [12] Xueyang Fu, Jiabin Huang, Xinghao Ding, Yinghao Liao, and John Paisley. Clearing the skies: A deep network architecture for single-image rain removal. *IEEE Transactions on Image Processing*, 26(6):2944–2956, 2017. 2
- [13] Xueyang Fu, Jiabin Huang, Delu Zeng, Yue Huang, Xinghao Ding, and John Paisley. Removing rain from single images via a deep detail network. In *Proceedings of the IEEE conference on computer vision and pattern recognition*, pages 3855–3863, 2017. 2
- [14] Chun-Le Guo, Qixin Yan, Saeed Anwar, Runmin Cong, Wenqi Ren, and Chongyi Li. Image dehazing transformer with transmission-aware 3d position embedding. In *Proceedings of the IEEE/CVF conference on computer vision and pattern recognition*, pages 5812–5820, 2022. 2
- [15] Kaiming He, Jian Sun, and Xiaoou Tang. Single image haze removal using dark channel prior. *IEEE transactions on pattern analysis and machine intelligence*, 33(12):2341–2353, 2010. 2
- [16] Jonathan Ho, Ajay Jain, and Pieter Abbeel. Denoising diffusion probabilistic models. *Advances in neural information processing systems*, 33:6840–6851, 2020. 2
- [17] Jia-Bin Huang, Abhishek Singh, and Narendra Ahuja. Single image super-resolution from transformed self-exemplars. In *Proceedings of the IEEE conference on computer vision and pattern recognition*, pages 5197–5206, 2015. 4, 5
- [18] Xiaozhong Ji, Yun Cao, Ying Tai, Chengjie Wang, Jilin Li, and Feiyue Huang. Real-world super-resolution via kernel estimation and noise injection. In *proceedings of the IEEE/CVF conference on computer vision and pattern recognition workshops*, pages 466–467, 2020. 5, 7
- [19] Kui Jiang, Zhongyuan Wang, Peng Yi, Chen Chen, Baojin Huang, Yimin Luo, Jiayi Ma, and Junjun Jiang. Multi-scale progressive fusion network for single image deraining. In *Proceedings of the IEEE/CVF conference on computer vision and pattern recognition*, pages 8346–8355, 2020. 5
- [20] Yuming Jiang, Kelvin CK Chan, Xintao Wang, Chen Change Loy, and Ziwei Liu. Reference-based image and video super-resolution via c^2 -matching. *IEEE Transactions on Pattern Analysis and Machine Intelligence*, 45(7):8874–8887, 2022. 6
- [21] Christian Ledig, Lucas Theis, Ferenc Huszár, Jose Caballero, Andrew Cunningham, Alejandro Acosta, Andrew Aitken, Alykhan Tejani, Johannes Totz, Zehan Wang, et al. Photo-realistic single image super-resolution using a generative adversarial network. In *Proceedings of the IEEE conference on computer vision and pattern recognition*, pages 4681–4690, 2017. 6
- [22] Jaewon Lee and Kyong Hwan Jin. Local texture estimator for implicit representation function. In *Proceedings of the IEEE/CVF conference on computer vision and pattern recognition*, pages 1929–1938, 2022. 2
- [23] Stamatios Lefkimmiatis. Universal denoising networks: a novel cnn architecture for image denoising. In *Proceedings of the IEEE conference on computer vision and pattern recognition*, pages 3204–3213, 2018. 2
- [24] Boyi Li, Wenqi Ren, Dengpan Fu, Dacheng Tao, Dan Feng, Wenjun Zeng, and Zhangyang Wang. Benchmarking single-image dehazing and beyond. *IEEE Transactions on Image Processing*, 28(1):492–505, 2018. 5
- [25] Boyun Li, Xiao Liu, Peng Hu, Zhongqin Wu, Jiancheng Lv, and Xi Peng. All-in-one image restoration for unknown corruption. In *Proceedings of the IEEE/CVF conference on computer vision and pattern recognition*, pages 17452–17462, 2022. 4, 5, 7

- [26] Ruoteng Li, Loong-Fah Cheong, and Robby T Tan. Heavy rain image restoration: Integrating physics model and conditional adversarial learning. In *Proceedings of the IEEE/CVF conference on computer vision and pattern recognition*, pages 1633–1642, 2019. 2
- [27] Yangming Li and Mihaela van der Schaar. On error propagation of diffusion models. In *The Twelfth International Conference on Learning Representations*, 2023. 1, 3, 7, 8
- [28] Yi Li, Yi Chang, Yan Gao, Changfeng Yu, and Luxin Yan. Physically disentangled intra-and inter-domain adaptation for varicolored haze removal. In *Proceedings of the IEEE/CVF Conference on Computer Vision and Pattern Recognition*, pages 5841–5850, 2022. 2
- [29] Yawei Li, Yuchen Fan, Xiaoyu Xiang, Denis Demandolx, Rakesh Ranjan, Radu Timofte, and Luc Van Gool. Efficient and explicit modelling of image hierarchies for image restoration. In *Proceedings of the IEEE/CVF Conference on Computer Vision and Pattern Recognition*, pages 18278–18289, 2023. 2
- [30] Jingyun Liang, Jiezhong Cao, Guolei Sun, Kai Zhang, Luc Van Gool, and Radu Timofte. Swinir: Image restoration using swin transformer. In *Proceedings of the IEEE/CVF international conference on computer vision*, pages 1833–1844, 2021. 2, 4, 5, 6, 7
- [31] Bee Lim, Sanghyun Son, Heewon Kim, Seungjun Nah, and Kyoung Mu Lee. Enhanced deep residual networks for single image super-resolution. In *Proceedings of the IEEE conference on computer vision and pattern recognition workshops*, pages 136–144, 2017. 2
- [32] Jingbo Lin, Zhilu Zhang, Yuxiang Wei, Dongwei Ren, Dongsheng Jiang, Qi Tian, and Wangmeng Zuo. Improving image restoration through removing degradations in textual representations. In *Proceedings of the IEEE/CVF Conference on Computer Vision and Pattern Recognition*, pages 2866–2878, 2024. 2
- [33] Yali Liu, Cherita Corbett, Ken Chiang, Rennie Archibald, Biswanath Mukherjee, and Dipak Ghosal. Sidd: A framework for detecting sensitive data exfiltration by an insider attack. In *2009 42nd Hawaii international conference on system sciences*, pages 1–10. IEEE, 2009. 5
- [34] Yuhao Liu, Zhanghan Ke, Fang Liu, Nanxuan Zhao, and Rynson WH Lau. Diff-plugin: Revitalizing details for diffusion-based low-level tasks. In *Proceedings of the IEEE/CVF Conference on Computer Vision and Pattern Recognition*, pages 4197–4208, 2024. 1, 2, 4, 5, 7
- [35] Liying Lu, Wenbo Li, Xin Tao, Jiangbo Lu, and Jiaya Jia. Masa-sr: Matching acceleration and spatial adaptation for reference-based image super-resolution. In *Proceedings of the IEEE/CVF Conference on Computer Vision and Pattern Recognition*, pages 6368–6377, 2021. 6
- [36] LiPing Lu, Qian Xiong, Bingrong Xu, and Duanfeng Chu. Mixdehazenet: Mix structure block for image dehazing network. In *2024 International Joint Conference on Neural Networks (IJCNN)*, pages 1–10. IEEE, 2024. 5
- [37] Ziwei Luo, Fredrik K Gustafsson, Zheng Zhao, Jens Sjölund, and Thomas B Schön. Photo-realistic image restoration in the wild with controlled vision-language models. In *Proceedings of the IEEE/CVF Conference on Computer Vision and Pattern Recognition*, pages 6641–6651, 2024. 4, 5, 7
- [38] Seungjun Nah, Tae Hyun Kim, and Kyoung Mu Lee. Deep multi-scale convolutional neural network for dynamic scene deblurring. In *Proceedings of the IEEE conference on computer vision and pattern recognition*, pages 3883–3891, 2017. 2
- [39] Zanlin Ni, Yulin Wang, Renping Zhou, Jiayi Guo, Jinyi Hu, Zhiyuan Liu, Shiji Song, Yuan Yao, and Gao Huang. Revisiting non-autoregressive transformers for efficient image synthesis. In *Proceedings of the IEEE/CVF Conference on Computer Vision and Pattern Recognition*, pages 7007–7016, 2024. 2
- [40] V Potlapalli, SW Zamir, S Khan, and FS Khan. Promptir: Prompting for all-in-one blind image restoration. *arXiv preprint arXiv:2306.13090*, 2023. 4, 5, 7
- [41] Wenqi Ren, Lin Ma, Jiawei Zhang, Jinshan Pan, Xiaochun Cao, Wei Liu, and Ming-Hsuan Yang. Gated fusion network for single image dehazing. In *Proceedings of the IEEE conference on computer vision and pattern recognition*, pages 3253–3261, 2018. 2
- [42] Robin Rombach, Andreas Blattmann, Dominik Lorenz, Patrick Esser, and Björn Ommer. High-resolution image synthesis with latent diffusion models. In *Proceedings of the IEEE/CVF conference on computer vision and pattern recognition*, pages 10684–10695, 2022. 2, 7
- [43] Chitwan Saharia, William Chan, Saurabh Saxena, Lala Li, Jay Whang, Emily L Denton, Kamyar Ghasemipour, Raphael Gontijo Lopes, Burcu Karagol Ayan, Tim Salimans, et al. Photorealistic text-to-image diffusion models with deep language understanding. *Advances in neural information processing systems*, 35:36479–36494, 2022. 2
- [44] Tim Salimans and Jonathan Ho. Progressive distillation for fast sampling of diffusion models. *arXiv preprint arXiv:2202.00512*, 2022. 2
- [45] Jiaming Song, Chenlin Meng, and Stefano Ermon. Denoising diffusion implicit models. *arXiv preprint arXiv:2010.02502*, 2020. 2
- [46] Yuda Song, Zhuqing He, Hui Qian, and Xin Du. Vision transformers for single image dehazing. *IEEE Transactions on Image Processing*, 32:1927–1941, 2023. 5
- [47] Ziyi Sun, Yunfeng Zhang, Fangxun Bao, Ping Wang, Xunxiang Yao, and Caiming Zhang. Sadnet: Semi-supervised single image dehazing method based on an attention mechanism. *ACM Transactions on Multimedia Computing, Communications, and Applications (TOMM)*, 18(2):1–23, 2022. 4
- [48] Stanislaw Szymanowicz, Christian Rupprecht, and Andrea Vedaldi. Splatter image: Ultra-fast single-view 3d reconstruction. In *Proceedings of the IEEE/CVF Conference on Computer Vision and Pattern Recognition*, pages 10208–10217, 2024. 2
- [49] Fu-Jen Tsai, Yan-Tsung Peng, Yen-Yu Lin, Chung-Chi Tsai, and Chia-Wen Lin. Stripformer: Strip transformer for fast image deblurring. In *European conference on computer vision*, pages 146–162. Springer, 2022. 2
- [50] Fu-Jen Tsai, Yan-Tsung Peng, Chung-Chi Tsai, Yen-Yu Lin, and Chia-Wen Lin. Banet: a blur-aware attention network

- for dynamic scene deblurring. *IEEE Transactions on Image Processing*, 31:6789–6799, 2022. 2
- [51] Zhengzhong Tu, Hossein Talebi, Han Zhang, Feng Yang, Peyman Milanfar, Alan Bovik, and Yinxiao Li. Maxim: Multi-axis mlp for image processing. In *Proceedings of the IEEE/CVF conference on computer vision and pattern recognition*, pages 5769–5780, 2022. 4, 5, 7
- [52] Jeya Maria Jose Valanarasu, Rajeev Yasarla, and Vishal M Patel. Transweather: Transformer-based restoration of images degraded by adverse weather conditions. In *Proceedings of the IEEE/CVF Conference on Computer Vision and Pattern Recognition*, pages 2353–2363, 2022. 2
- [53] Cong Wang, Jinshan Pan, Wei Wang, Jiangxin Dong, Mengzhu Wang, Yakun Ju, and Junyang Chen. Promptrestorer: A prompting image restoration method with degradation perception. *Advances in Neural Information Processing Systems*, 36:8898–8912, 2023. 2
- [54] Jianyi Wang, Zongsheng Yue, Shangchen Zhou, Kelvin CK Chan, and Chen Change Loy. Exploiting diffusion prior for real-world image super-resolution. *International Journal of Computer Vision*, pages 1–21, 2024. 2, 7
- [55] Tengfei Wang, Jiabin Xie, Wenxiu Sun, Qiong Yan, and Qifeng Chen. Dual-camera super-resolution with aligned attention modules. In *Proceedings of the IEEE/CVF International Conference on Computer Vision*, pages 2001–2010, 2021. 2, 5, 6, 7
- [56] Xintao Wang, Liangbin Xie, Chao Dong, and Ying Shan. Real-esrgan: Training real-world blind super-resolution with pure synthetic data. In *Proceedings of the IEEE/CVF international conference on computer vision*, pages 1905–1914, 2021. 6, 7
- [57] Yufei Wang, Wenhan Yang, Xinyuan Chen, Yaohui Wang, Lanqing Guo, Lap-Pui Chau, Ziwei Liu, Yu Qiao, Alex C Kot, and Bihan Wen. Sinsr: diffusion-based image super-resolution in a single step. In *Proceedings of the IEEE/CVF Conference on Computer Vision and Pattern Recognition*, pages 25796–25805, 2024. 2
- [58] Zhendong Wang, Xiaodong Cun, Jianmin Bao, Wengang Zhou, Jianzhuang Liu, and Houqiang Li. Uformer: A general u-shaped transformer for image restoration. In *Proceedings of the IEEE/CVF conference on computer vision and pattern recognition*, pages 17683–17693, 2022. 2
- [59] Zejin Wang, Jiazheng Liu, Guoqing Li, and Hua Han. Blind2unblind: Self-supervised image denoising with visible blind spots. In *Proceedings of the IEEE/CVF conference on computer vision and pattern recognition*, pages 2027–2036, 2022. 4
- [60] Jay Whang, Mauricio Delbracio, Hossein Talebi, Chitwan Saharia, Alexandros G Dimakis, and Peyman Milanfar. Deblurring via stochastic refinement. In *Proceedings of the IEEE/CVF Conference on Computer Vision and Pattern Recognition*, pages 16293–16303, 2022. 2
- [61] Jia-Hao Wu, Fu-Jen Tsai, Yan-Tsung Peng, Chung-Chi Tsai, Chia-Wen Lin, and Yen-Yu Lin. Id-blau: Image deblurring by implicit diffusion-based reblurring augmentation. In *Proceedings of the IEEE/CVF Conference on Computer Vision and Pattern Recognition*, pages 25847–25856, 2024. 2
- [62] Rongyuan Wu, Tao Yang, Lingchen Sun, Zhengqiang Zhang, Shuai Li, and Lei Zhang. Seesr: Towards semantics-aware real-world image super-resolution. In *Proceedings of the IEEE/CVF conference on computer vision and pattern recognition*, pages 25456–25467, 2024. 2, 7
- [63] Bin Xia, Yulun Zhang, Shiyin Wang, Yitong Wang, Xinglong Wu, Yapeng Tian, Wenming Yang, and Luc Van Gool. Diffir: Efficient diffusion model for image restoration. In *Proceedings of the IEEE/CVF International Conference on Computer Vision*, pages 13095–13105, 2023. 2, 7
- [64] Jie Xiao, Xueyang Fu, Aiping Liu, Feng Wu, and Zheng-Jun Zha. Image de-raining transformer. *IEEE Transactions on Pattern Analysis and Machine Intelligence*, 45(11):12978–12995, 2022. 2
- [65] Kang Xu, Weixin Li, Xia Wang, Xiaoyan Hu, Ke Yan, Xiaojie Wang, and Xuan Dong. Cur transformer: A convolutional unbiased regional transformer for image denoising. *ACM Transactions on Multimedia Computing, Communications and Applications*, 19(3):1–22, 2023. 2
- [66] Ruikang Xu, Mingde Yao, and Zhiwei Xiong. Zero-shot dual-lens super-resolution. In *Proceedings of the IEEE/CVF Conference on Computer Vision and Pattern Recognition*, pages 9130–9139, 2023. 6
- [67] Fuzhi Yang, Huan Yang, Jianlong Fu, Hongtao Lu, and Baining Guo. Learning texture transformer network for image super-resolution. In *Proceedings of the IEEE/CVF conference on computer vision and pattern recognition*, pages 5791–5800, 2020. 2, 6
- [68] Jianchao Yang, John Wright, Thomas S Huang, and Yi Ma. Image super-resolution via sparse representation. *IEEE transactions on image processing*, 19(11):2861–2873, 2010. 2
- [69] Dongjie Ye, Zhangkai Ni, Hanli Wang, Jian Zhang, Shiqi Wang, and Sam Kwong. Csformer: Bridging convolution and transformer for compressive sensing. *IEEE Transactions on Image Processing*, 32:2827–2842, 2023. 2
- [70] Tian Ye, Sixiang Chen, Wenhao Chai, Zhaohu Xing, Jing Qin, Ge Lin, and Lei Zhu. Learning diffusion texture priors for image restoration. In *Proceedings of the IEEE/CVF Conference on Computer Vision and Pattern Recognition*, pages 2524–2534, 2024. 2
- [71] Fanghua Yu, Jinjin Gu, Zheyuan Li, Jinfan Hu, Xiangtao Kong, Xintao Wang, Jingwen He, Yu Qiao, and Chao Dong. Scaling up to excellence: Practicing model scaling for photo-realistic image restoration in the wild. In *Proceedings of the IEEE/CVF Conference on Computer Vision and Pattern Recognition*, pages 25669–25680, 2024. 2
- [72] Huanjing Yue, Zifan Cui, Kun Li, and Jingyu Yang. Kedusr: Real-world dual-lens super-resolution via kernel-free matching. In *Proceedings of the AAAI Conference on Artificial Intelligence*, pages 6881–6889, 2024. 2, 6
- [73] Zongsheng Yue, Jianyi Wang, and Chen Change Loy. Resshift: Efficient diffusion model for image super-resolution by residual shifting. *Advances in Neural Information Processing Systems*, 36, 2024. 1, 2, 3, 7
- [74] Syed Waqas Zamir, Aditya Arora, Salman Khan, Munawar Hayat, Fahad Shahbaz Khan, and Ming-Hsuan Yang.

- Restormer: Efficient transformer for high-resolution image restoration. In *Proceedings of the IEEE/CVF conference on computer vision and pattern recognition*, pages 5728–5739, 2022. 2, 4, 5, 7
- [75] Lvmin Zhang, Anyi Rao, and Maneesh Agrawala. Adding conditional control to text-to-image diffusion models. In *Proceedings of the IEEE/CVF International Conference on Computer Vision*, pages 3836–3847, 2023. 2
- [76] Wenlong Zhang, Xiaohui Li, Guangyuan Shi, Xiangyu Chen, Yu Qiao, Xiaoyun Zhang, Xiao-Ming Wu, and Chao Dong. Real-world image super-resolution as multi-task learning. *Advances in Neural Information Processing Systems*, 36, 2024. 2
- [77] Yulun Zhang, Kunpeng Li, Kai Li, Lichen Wang, Bineng Zhong, and Yun Fu. Image super-resolution using very deep residual channel attention networks. In *Proceedings of the European conference on computer vision (ECCV)*, pages 286–301, 2018. 2
- [78] Yi Zhang, Dasong Li, Xiaoyu Shi, Dailan He, Kangning Song, Xiaogang Wang, Hongwei Qin, and Hongsheng Li. Kbnet: Kernel basis network for image restoration. *arXiv preprint arXiv:2303.02881*, 2023. 4, 5
- [79] Zhifei Zhang, Zhaowen Wang, Zhe Lin, and Hairong Qi. Image super-resolution by neural texture transfer. In *Proceedings of the IEEE/CVF conference on computer vision and pattern recognition*, pages 7982–7991, 2019. 6
- [80] Zhilu Zhang, Ruohao Wang, Hongzhi Zhang, Yunjin Chen, and Wangmeng Zuo. Self-supervised learning for real-world super-resolution from dual zoomed observations. In *European Conference on Computer Vision*, pages 610–627. Springer, 2022. 2, 6
- [81] Shihao Zhao, Dongdong Chen, Yen-Chun Chen, Jianmin Bao, Shaozhe Hao, Lu Yuan, and Kwan-Yee K Wong. Uni-controlnet: All-in-one control to text-to-image diffusion models. *Advances in Neural Information Processing Systems*, 36, 2024. 2
- [82] Dian Zheng, Xiao-Ming Wu, Shuzhou Yang, Jian Zhang, Jian-Fang Hu, and Wei-Shi Zheng. Selective hourglass mapping for universal image restoration based on diffusion model. In *Proceedings of the IEEE/CVF Conference on Computer Vision and Pattern Recognition*, pages 25445–25455, 2024. 1, 2, 4, 5, 7
- [83] Yupeng Zhou, Zhen Li, Chun-Le Guo, Song Bai, Ming-Ming Cheng, and Qibin Hou. Srformer: Permuted self-attention for single image super-resolution. In *Proceedings of the IEEE/CVF International Conference on Computer Vision*, pages 12780–12791, 2023. 2, 7
- [84] Yurui Zhu, Tianyu Wang, Xueyang Fu, Xuanyu Yang, Xin Guo, Jifeng Dai, Yu Qiao, and Xiaowei Hu. Learning weather-general and weather-specific features for image restoration under multiple adverse weather conditions. In *Proceedings of the IEEE/CVF conference on computer vision and pattern recognition*, pages 21747–21758, 2023. 2, 5
- [85] Yuanzhi Zhu, Kai Zhang, Jingyun Liang, Jiezhang Cao, Bihan Wen, Radu Timofte, and Luc Van Gool. Denoising diffusion models for plug-and-play image restoration. In *Proceedings of the IEEE/CVF Conference on Computer Vision and Pattern Recognition*, pages 1219–1229, 2023. 2
- [86] Yixuan Zhu, Wenliang Zhao, Ao Li, Yansong Tang, Jie Zhou, and Jiwen Lu. Flowie: Efficient image enhancement via rectified flow. In *Proceedings of the IEEE/CVF Conference on Computer Vision and Pattern Recognition*, pages 13–22, 2024. 2